

See discussions, stats, and author profiles for this publication at: <https://www.researchgate.net/publication/236213508>

Stretch-Induced Crystal–Crystal Transition of Polybutene-1: An in Situ Synchrotron Radiation Wide-Angle X-ray Scattering Study

ARTICLE in MACROMOLECULES · MARCH 2012

Impact Factor: 5.8 · DOI: 10.1021/ma2026513

CITATIONS

22

READS

63

8 AUTHORS, INCLUDING:



Kunpeng Cui

Hokkaido University

21 PUBLICATIONS 136 CITATIONS

[SEE PROFILE](#)



Liangbin Li

University of Science and Technology of China

137 PUBLICATIONS 2,046 CITATIONS

[SEE PROFILE](#)



Zhe Ma

Technische Universiteit Eindhoven

44 PUBLICATIONS 371 CITATIONS

[SEE PROFILE](#)

Stretch-Induced Crystal–Crystal Transition of Polybutene-1: An in Situ Synchrotron Radiation Wide-Angle X-ray Scattering Study

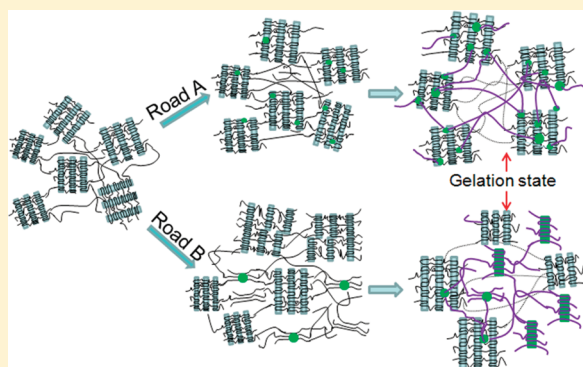
Yanping Liu,[†] Kunpeng Cui,[†] Nan Tian,[†] Weiqing Zhou,[†] Lingpu Meng,[†] Liangbin Li,^{*,†} Zhe Ma,[‡] and Xiaolin Wang[§]

[†]National Synchrotron Radiation Lab and College of Nuclear Science and Technology, CAS Key Laboratory of Soft Matter Chemistry, University of Science and Technology of China, Hefei, China

[‡]Materials Technology, Eindhoven University of Technology, Eindhoven, The Netherlands

[§]Chinese Academy of Engineering Physics, Mianyang, China

ABSTRACT: Deformation induced crystal–crystal transition of polybutene-1 (PB-1) from forms II to I at different temperatures is studied with in situ synchrotron radiation wide-angle X-ray scattering (WAXS). Analyses on the evolution of crystallinity and orientations of forms II and I during tensile deformation show that stretch accelerates the transformation from forms II to I, which is interpreted based on either a direct crystal–crystal transition or an indirect approach via an intermediate state of melt, namely a melting recrystallization process. A three-stage mechanical deformation including linear deformation, stress plateau, and strain hardening is observed in the engineering stress–strain curves, which corresponds to a process of incubation, nucleation, and gelation of form I crystals. It establishes a nice correlation between phase transition and mechanical behavior in this study.



INTRODUCTION

The structure–mechanical property relationship of semicrystalline polymer materials is a long-standing challenge in polymer academic and industrial communities. For semicrystalline polymers composed of multiscale structures from monomer composition, lamellar crystal to spherulite, it is formidably difficult to correlate macroscopic mechanical property with microstructures at different length scales. Additionally, during tensile or other mechanical deformation, external force may induce complicated structural and morphological changes like solid–solid and liquid–solid transitions, which will lead to a feedback on the mechanical property and leave their signatures on the stress–strain curves.^{1–5} During deformation, the structural evolution and mechanical property are dynamically coupled with each other, and in situ measurements combining structure and property characterizing techniques become essential on understanding structure and mechanical property relations of those materials. Indeed combining an in situ tensile tester with synchrotron radiation X-ray scattering techniques provides rich structure–property information for many semicrystalline polymers.^{6–9} New phases were reported during deformation of polymers, like the mesophase of poly(ethylene terephthalate),^{6,10–12} the conformation disordered hexagonal crystal in polyethylene (PE),¹³ and the transient α'' phase found in polyamide.^{14,15} Solid–solid phase transition may even lead to unique mechanical property, like the superelasticity of syndiotactic polypropylene (sPP) which is attributed to deformation-induced martensitic-like crystal–crystal transi-

tion.^{16,17} Moreover, in the case of isotactic polypropylene (iPP), the transformation from α or γ crystals into the mesophase may bring various degree of mechanical properties ranging between stiff and elastomeric.^{18–21}

Polybutene-1(PB-1) is a commercially interesting polyolefin because of its wide applications, like hot water pipes, pressurized tanks and tubes. However, applications of PB-1 are limited comparing with other polyolefins like polypropylene and polyethylene. In addition to slightly higher cost of the raw material, the complication of crystal–crystal transition is also an important consideration. The solid phase transition may bring undesirable effect, such as shrinkage of the molded objects caused by densification.^{22,23} PB-1 exhibits multiphases depending on the crystallization condition: form I, twined hexagonal with a 3_1 helix; form I', untwined hexagonal with a 3_1 helix; form II, tetragonal with an 11_3 helix; form II', tetragonal structure; form III, orthorhombic with a 4_1 helix.^{24–27} Form II is a metastable structure which forms when the polymer crystallizes from melt at atmospheric pressure, and which transforms into the thermodynamically stable form I when held at room temperature. Depending on the environmental condition, the transformation may take several weeks to finish, during which the material properties are changed profoundly.^{22,28} With the help of tensile deformation, the

Received: December 7, 2011

Revised: March 8, 2012

Published: March 15, 2012



transformation process will be accelerated.²⁹ After the transformation, the melting point increases to 135 °C of form I from 117 °C of form II. Besides that, the material will become rigid and display higher strength.^{30–33} In order to shorten the transition time, recent work have been tried to obtain form I crystal directly under peculiar condition, like ultrathin film,³⁴ self-seeding³⁵ and different concentration of stereodefects.³⁶ Form III and form I' have been found to form in solution crystallization, depending on the solvent, concentration and the crystallization temperature.^{37–39} At higher temperature, both forms III and I' first transform into form II by the aid of drawing, and then into form I.⁴⁰

Because of the industrial and academic interests, the transformation from forms II to I has been extensively studied in the past decades.^{41–48} It has been reported that this transformation is a nucleation-controlled process with nuclei localized at lamellar distortion points or the crystal surfaces or corners.³⁹ Based on X-ray and electron diffraction studies, Fujiwara et al.⁴⁹ and Kopp et al.⁵⁰ suggest that the (110) plane of form II tetragonal crystal becomes the same plane of form I hexagonal crystal. In this way, the helix displacement is minimized and the energetically unrealistic change of helix chirality is avoided. The transition kinetics is strongly dependent on the initial crystallization temperature and circumstance. High pressure^{28,51} or pressured CO₂,^{52,53} deformation^{54–56} and additives like plasticizers or nucleating agents⁵⁷ are reported to accelerate the transition kinetics. Deformation assisted forms II to I transition of PB-1 has been studied since 1960s.⁵⁸ A strong effect of strain on the transformation was reported by Goldbach et al.,⁵⁹ where the importance of strain on the amorphous chains was emphasized as amorphous relaxation counteracted the accelerating effect. During stretch induced transition from forms II to I of PB-1, an unusual two-stage strain hardening was observed by Yang et al.⁶⁰ Though the accelerating effect of deformation on crystal–crystal transition from forms II to I is well recognized, no direct correlation between structure and mechanical property is established yet.

For the purpose of correlating the phase transformation with mechanical properties of PB-1, the phase transition of commercial grade sample during uniaxial tensile deformation is studied with in situ synchrotron radiation wide-angle X-ray scattering. Two transition points are observed on the engineering stress–strain curves, which correspond to nucleation of form I crystal and gelation of form I mechanical network, respectively. The transition from forms II to I follows two different routes, namely a direct crystal–crystal transition and a melting recrystallization process.

■ EXPERIMENTAL SECTION

The tensile test was carried out on a homemade miniature mechanical tester, which was equipped with a temperature controlled oven with nitrogen purge. Error of the force sensor of the apparatus was less than 1 N. The uniaxial tensile tests were performed at several designated temperatures (25, 50, and 80 °C) and the drawing speed was fixed at 3.15 mm/min. After the dumbbell shaped sample was mounted between two clamps of the tester with an initial length of 10 mm, temperature was increased to the designated temperature in 5 min. When the temperature was stabilized for 5 min, stretch was imposed on the sample. The change of sample width was followed with a high precision CCD camera.

In-situ WAXS measurements were carried out on synchrotron radiation X-ray scattering station with a radiation wavelength of 0.154 nm and Mar 345 image plate as a detector in National Synchrotron

Radiation Laboratory (NSRL), Hefei, China. The sample-to-detector distance for WAXS was 323 mm. Fit2D software package was used to analyze the two-dimensional (2D) WAXS patterns. Air background was subtracted in the 2D scattering patterns.

PB-1 granules are kindly supplied by LyondellBasell Industries with a trade name of PB0110M, which has with a molecular weight $M_w = 711000$ g/mol and $M_w/M_n = 3.1$. The melting point and glass transition temperature are about 117 and –20 °C, respectively. The PB-1 plates with a thickness of 1 mm were first made through compression molding. For tensile testing, the plates were further cut into dumbbell shaped samples, with length and width of 29 and 4 mm, respectively. The samples were heated to 170 °C and held for 5 min to erase the processing history, then cooled to the crystallization temperatures 85, 95, 105 °C at a cooling rate of 9 °C/min. At the crystallization temperature of 85 and 95 °C, the samples were held isothermally for more than 40 min to crystallize completely. Because of the slow crystallization rate at 105 °C, the samples were held for more than 3 h. After complete crystallization, the samples were quickly mounted on the tester to carry out tensile experiments. No diffraction signal of form I was detected before uniaxial drawing.

■ RESULTS

According to the crystallization condition adopted in the sample preparation, the crystal phase in the PB-1 samples before tensile test is the metastable form II, which is also verified by the WAXS patterns. The three main diffraction peaks are observed at 2θ of about 11.8, 16.9, and 18.4°, which correspond to crystallographic planes (200), (220), and (213) of form II crystal, respectively.

Figure 1a depicts the engineering stress–strain curve (ESSC) of PB-1 during tensile test at room temperature (25 °C controlled by air condition), which was initially crystallized at 95 °C. Several selected two-dimensional (2D) WAXS patterns at various strain levels are inserted. The tensile deformation is

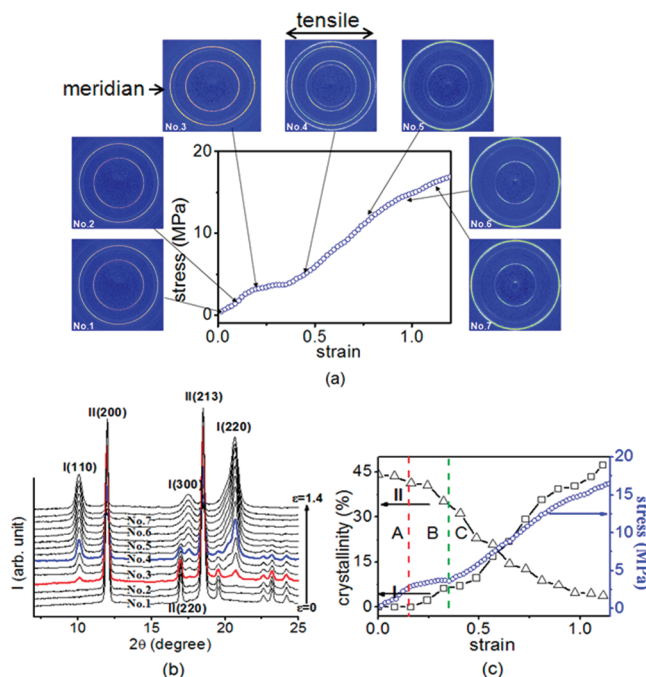


Figure 1. (a) Engineering stress–strain curve and the selected WAXS patterns during uniaxial tensile deformation at room temperature. (b) Corresponding one-dimensional WAXS curves. (c) Crystallinity of forms I and II calculated from part b in conjunction with the corresponding engineering stress–strain curve. The crystallization temperature (T_c) for this sample is 95 °C.

along horizontal direction. Before stretching, the diffraction peaks with relatively strong intensity of crystal planes (200), (220) and (213) of form II crystal are clearly viewed in the 2D WAXS patterns. Upon increasing strain to the yield point, deformation-induced orientation of crystals can be easily visualized in 2D WAXS patterns, while the appearance of more diffraction peaks indicates the formation of new crystal structure.

To present detailed evolution of phase transformation, the integrated one-dimensional (1D) WAXS curves during the tensile test are shown in Figure 1b. Three new diffraction peaks appear on 1D WAXS curves clearly when the engineering strain reaches about 0.2 (indicated by red line), which correspond to the crystallographic planes (110), (300), (220) of form I. These peak intensities of form I increase with strain, while that of form II decrease and finally die away. A quantitative analysis on the deformation induced crystal-crystal transition of forms II to I is presented in Figure 1c, where we plot the crystallinity of forms I and II during deformation. The corresponding ESSC is also plotted in Figure 1c for a direct correlation between structure and mechanical property. The evolution of the phase transition can be divided into three stages, which are separated by the red and green dash lines in Figure 1c. In stage A, no diffraction signal from form I can be detected, indicating that the transformation from forms II to I does not start yet. Stage A matches well with the linear deformation region as indicated by ESSC. Following the linear region, the ESSC enters into a stress plateau-like region, which is defined as stage B. Coincidentally, form I appears exactly at the beginning of the stress plateau. The onset of the engineering stress plateau is essentially a mechanical yield, which suggests that the beginning of transition from forms II to I, or nucleation of form I corresponds to the yield of form II crystals. In stage B, the crystallinity of form I keeps at a low level though it still increases continuously. At the end of the engineering stress plateau region, the crystallinity reaches about 6%. Analogue to isothermal crystallization, if we define stage A as the induction period of crystallization, stage B is rather similar to the nucleation period. Stage C starts at the end of the stress plateau and the stress increases nearly linearly with strain again, which is a strain hardening region. Here the transition from forms II to I is accelerated, which may correspond to the growth stage of form I.

It is interesting to note that a slowdown of the transformation seems to exist at the beginning of stage C though the overall increase of the crystallinity of form I is rapid in this stage. In order to have a better view, we plot the crystallinity of form I in the true stress-true strain diagram during tensile deformation in Figure 2. Indeed a slowdown of the transformation rate from forms II to I accompanies with the stress level-up or strain hardening after the plateau region. Evidently

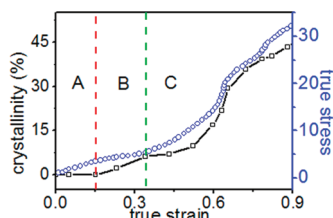


Figure 2. Crystallinity evolution of form I combining with the corresponding true stress-strain curve.

the strain hardening in stage C is due to the formation of a new mechanical network constructed by form I. The formation of the new mechanical network may take major share of stress, which releases form II from stress partially and consequently slows down the transformation. This will be discussed in more detail in the Discussion.

Deformation-induced orientation of forms II and I during tensile test is analyzed through the azimuthal intensity distribution of (200) crystal plane of form II and (110) of form I, which are plotted in Figure 3, parts a and b, respectively. As mentioned above, in stage A, only form II crystals exist, which remains isotropic as indicated by the azimuthal intensity distribution of (200) plane of form II. When the deformation enters into stage B, the orientation of (200) planes of form II starts to shift into the 45° direction which may be the shear band.^{61–63} The coincidence between mechanical yield and crystal rotation is a general phenomenon in semicrystalline polymers.^{1,64} At the beginning of stage B, scattering intensity of form I crystal emerges, with the crystal plane (110) polarized on the equator, in other words with chain axis tending to be parallel to the tensile direction. The different orientation of forms I and II in stage B indicates that nucleation of form I and rotation of form II are two uncorrelated events, though both correlate with the mechanical yield during tensile deformation at room temperature. Further increasing tensile strain, the orientation of form I (110) shifts to 45° in stage C, which is same as that of form II (200). Here it is more like that the growth of form I consumes form II crystals that already oriented in this direction.

The same tensile experiments with in situ synchrotron radiation WAXS to follow structure evolution were further carried out on samples crystallized at 85 and 105 °C, respectively. For conciseness, we present the crystallinity evolution of forms II and I and the engineering stress-strain curves during tensile test in Figure 4, parts a and b, respectively. The ESSC and the crystallinity evolution of forms II and I for samples crystallized at 85 °C (Figure 4a) and 105 °C (Figure 4b) are essentially same as that crystallized at 95 °C, which confirms that the three-stage transformation process from forms II to I is a general feature of PB-1. Comparing with the samples crystallized at lower temperatures (85 and 95 °C), stage B for the sample crystallized at 105 °C seems to be shorter, which is possibly due to different crystallite forms when crystallized at different temperatures. It is reported that at low supercooling PB-1 crystallized into hemicrystalline structure, while at high supercooling spherulite is formed.⁴⁷ At the transition point between stages B and C, the crystallinity of form I always keeps at a relatively low level, which is less than 6% for both samples crystallized 85 and 105 °C. In general, within the temperature range we studied, initial crystallization temperature seems to play a weak role in the deformation induced crystal-crystal transition.

We further studied the effect of tensile deformation temperature on the crystal-crystal transition. Below the melting temperature of PB-1, in situ tensile deformation experiments on the sample crystallized at 95 °C were performed at 50 and 80 °C, respectively. As the overall trend of the engineering stress-strain curve and the evolution of forms II to I crystal-crystal transition at 50 °C is rather similar to that at room temperature, we only present data of 80 °C in Figure 5a. The ESSC can be divided into three regions which are same as that at low temperatures (separated by the red and green dash lines), but the specific structure evolution is

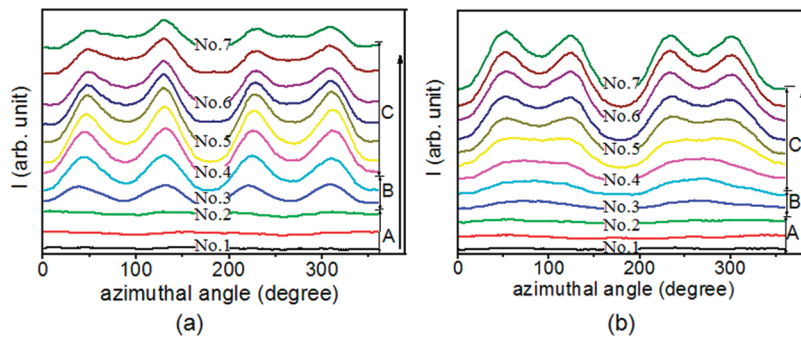


Figure 3. One-dimensional azimuthal intensity curves of (200) plane of form II (a) and (110) of form I (b) during deformation at room temperature with tensile direction in 0–180° (horizontal direction).

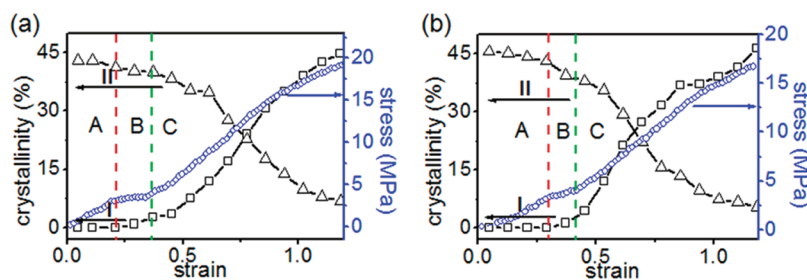


Figure 4. Crystallinity evolution of forms I and II in conjunction with the corresponding engineering stress–strain curves during deformation at 25 °C for the sample crystallized at temperatures of 85 °C (a) and 105 °C (b), respectively.

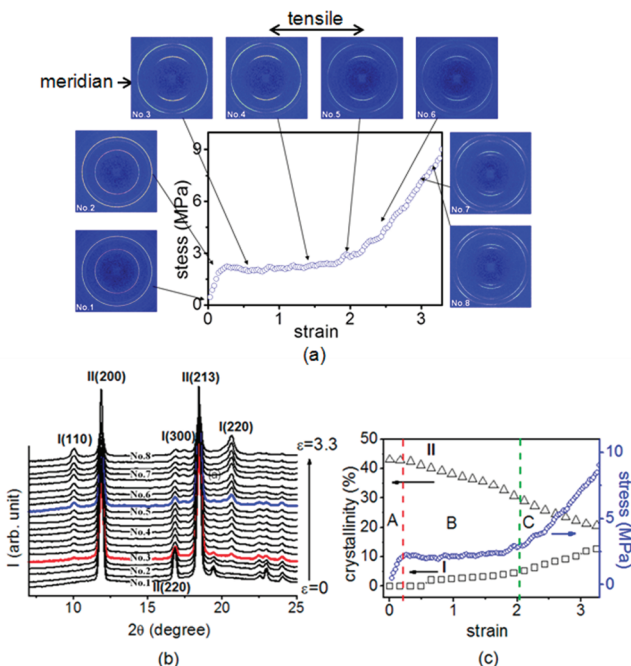


Figure 5. (a) Engineering stress–strain curve and the selected WAXS patterns during tensile deformation at 80 °C with $T_c = 95$ °C. (b) Corresponding one-dimensional WAXS curves. (c) Crystallinity evolution of forms I and II calculated from part b and the corresponding stress–strain curve.

different from that at low temperatures. At 80 °C, form I does not appear at the first turning point (yield point) on the ESSC where the engineering strain is 0.2, but emerges in the middle of the plateau region with a strain of 0.6. Note that the plateau (stage B) covers a broader strain range from 0.2 to 2.1. Figure 5b shows the integrated one-dimensional WAXS curves during

tensile deformation at 80 °C. The red curve corresponds to the first appearance of form I at the strain of 0.6, while the blue one corresponds to the second turning point or the onset of strain hardening. The diffraction intensity of form I is weaker than that of form II during the whole tensile deformation process as shown in Figure 5b. The crystallinity of both forms II and I are plotted versus engineering strain in Figure 5c, where the ESSC is also added for the convenience of correlating. In the stress plateau region (stage B), the crystal–crystal transformation from forms II to I is very slow and only 2% crystallinity of form I is generated at the end of the plateau region (Figure 5c). Interestingly, the crystallinity of form II declines obviously faster than the increase of that of form I, which suggests that the overall crystallinity of forms II and I in the sample decreases during the tensile deformation at 80 °C. In other words, part of form II melts rather than transforms to form I directly under stress at high temperature.

Parts a and b of Figures 6 show the azimuthal intensity distributions of the representative planes, crystal plane (200) of form II and (110) of form I, during tensile deformation at 80 °C for the whole process, respectively. In the linear deformation region (stage A), no obvious orientation of form II is observed (Figure 6a). As soon as the deformation enters into the stress plateau region (stage B), the (200) plane of form II starts to orient in about 50° direction. Further increasing strain, the azimuthal intensity of form II (200) shifts its maximum to about 68° at the strain of 0.6, where form I emerges. From the strain of 0.6 to the end of stage B (at strain of 2.1), the azimuthal intensity distribution of form II (200) keeps its peak position unchanged at 68°. In the strain hardening region (stage C) the orientation of form II (200) plane further shifts to meridian direction. On the other hand, the orientation of the crystallographic plane (110) of form I is along meridian direction from its first appearance at the strain

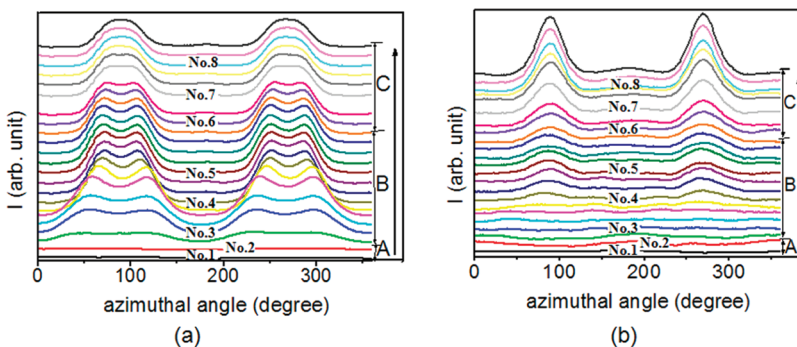


Figure 6. One-dimensional azimuthal intensity curves of (a) (200) plane of form II and (b) (110) plane of form I during uniaxial deformation at 80 °C with $T_c = 95$ °C. The tensile axis lies along the 0–180° direction, while 0° and 90° are meridian and equator, respectively.

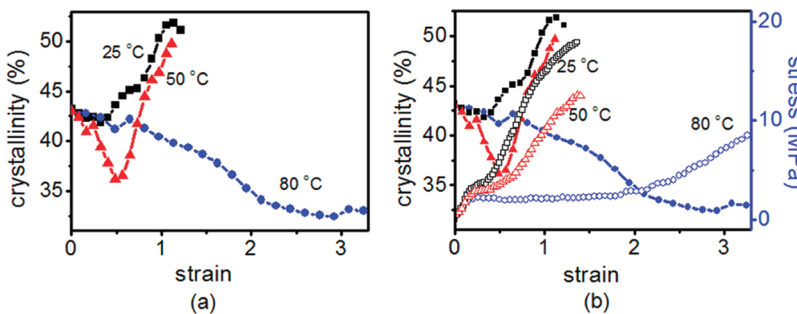


Figure 7. (a) Sum of the crystallinity (X_{II+I}) of forms II and I (solid symbol) (b) and the corresponding ESSC for different experimental temperatures 25, 50, and 80 °C (open symbol).

of 0.6, which keeps unchanged during the whole tensile deformation process.

Tensile deformation temperature does show significant influence on the phase transition. Instead of plotting crystallinity of forms II and I separately, here we plot the sum of their crystallinity during tensile deformation at different temperatures in Figure 7a, which is denoted as X_{II+I} for the convenience of description. As diffraction intensity is determined by many factors like structural factor, multiplicity factor, etc., Figure 7 only gives a semiquantitative trend of the overall mass or volume crystallinity. Note that the mass correction due to different densities of forms II and I does not affect the trends. In order to correlate the volume fractions of all solid crystals with the mechanical behaviors, the sum of crystallinity X_{II+I} are replotted together with the corresponding ESSCs in Figure 7b. At 25 °C, the sum of crystallinity X_{II+I} does not vary obviously in stages A and B, which levels up as entering the strain hardening region or stage C (see Figure 7b) and reaches a value of about 52%. On the contrary, tensile deformation at high temperature of 80 °C leads to a continuous decline of X_{II+I} , which reaches a low level of about 32%. At an intermediate temperature 50 °C, the evolution of X_{II+I} follows a nonmonotonic behavior, which first decreases in stages A and B to about 36%, and then increases back to about 50%. These three different evolution behaviors of X_{II+I} indicate that stress may induce form II crystal to melt at temperature below its melting point, while those molten amorphous part will crystallize into form I under further stretch, especially at intermediate temperatures as demonstrated at 50 °C. The evolution trends of the X_{II+I} correlate rather well with their corresponding ESSCs. The leveling up points of X_{II+I} at 25 and 50 °C locate exactly at the onset of stage C (strain hardening region). Though X_{II+I} does not show a leveling up at 80 °C, the

onset of strain hardening corresponds to a flattening of the decrease trend of X_{II+I} which may have the same physical mechanism as the leveling up at lower temperatures.

DISCUSSION

On the basis of in situ WAXS measurements during tensile deformation of PB-1, several interesting findings can be extracted. (i) The transformation from forms II to I is accelerated by uniaxial tensile deformation, which is suppressed with the increase of deformation temperature. (ii) During tensile deformation process, the sums of crystallinity X_{II+I} follow nearly monotonic increase and decrease with strain at 25 and 80 °C, respectively, while a nonmonotonic trend with first decrease and then increase process is observed at the intermediate temperature of 50 °C, which suggests that two different routes may exist in the transition from forms II to I. One is a direct transformation from the metastable form II to the stable form I at low temperature of 25 °C, which is similar to the phase transition at quiescent condition. The second occurs at high temperature of 80 °C, which is a process of deformation induced melting and recrystallization. (iii) Two interesting turning points have been found on the engineering stress-strain curves, which correspond to the specific structural transformations, respectively. At low temperature the transition from forms II to I begins at the first turning point (yield point). The second turning point indicates the onset of strain hardening, where a critical concentration of form I is generated to form a new mechanical network. Thus, this is a gelation point of the newly formed mechanical network with form I acting as the physical cross-link. Focusing on these points above, we will give some discussions in the following paragraphs.

The transformation from the metastable form II to the stable form I is accelerated largely by tensile deformation. In our experiments, the degree of phase transformation Φ reaches about 80% in 40 min at room temperature (Figure 1c and Figure 4, parts a and b). Here, the degree of phase transformation is defined as $\Phi = X_{\text{I}t} / X_{\text{II}0}$, where $X_{\text{I}t}$ is the crystallinity of form I at time t , and $X_{\text{II}0}$ is the crystallinity of form II before tensile deformation. However, it has been reported the transformation from forms II to I may take several weeks to finish under quiescent condition at room temperature.⁴⁴ When deformation is applied, the volumetric free energy difference between forms II and I is raised as $\Delta G = \Delta G_q + \Delta G_f$, where ΔG_q is the thermodynamic driving force at quiescent condition and ΔG_f is the driving force coming from external field like the stress in this work. Stress increases the free energy of form II and decreases the nucleation barrier of form I, which leads to an acceleration of the transformation from forms II to I. According to the transformation mechanism proposed by Fujiwara⁴⁹ and Lotz,⁵⁰ the (110) planes exist as an “invariant plane” (Figure 8a). Direct transition from tetragonal form II with 11_3 helix to trigonal form I with 3_1 helix gives a near-matching (-4%) of interhelical distance and preserves the chirality of helical planes, which seems to be an easy approach without large rearrangement of molecular units. In the normal direction of these planes, main part of the contraction takes place. Averagely, the interplanar distance is reduced by nearly 20% (see Figure 8a). The transformation is accelerated under tensile deformation via promoting the contraction. For example, in the vertical zone of Figure 8b, chains in the lamellae are parallel to the tensile direction. When the tensile stress σ_1 is applied on form II crystal, the stress σ_2 and σ_3 in the two directions perpendicular to σ_1 will assist the contraction of interhelix and interplanar distance of (110) planes respectively (see Figure 8b). Oppositely, in the horizontal zone, the stress parallel to the normal of (110) plane may play a negative role in contracting. This analysis is also consistent with the initial orientation of form I whose chain axis is along tensile direction.

The transition from forms II to I is delayed with the increase of temperature. Comparing with the result at lower temperatures, the transformation is much slower at 80 °C, where the transition degree Φ reaches less than 20% in 40 min (much less than 80% at room temperature). It has been reported that the phase transformation of PB-1 is a nucleation controlled process.⁶⁵ The nucleus of form I at quiescent condition is thought to be created mainly by thermal stresses, due to different thermal expansion coefficients of crystal and amorphous component. This thermal stress is prone to occur at regions with irregular stack of lamella, local variation of lamellar thickness, and bending of lamellae. At low temperature, tensile deformation amplifies local thermal stress and creates more sites for form I to nucleate, which behaves as a fast transition rate from forms II to I. On the other hand, higher temperature leads to faster relaxation of the thermal stress, which counteracts the acceleration effect of tensile deformation on the transition. Comparing with the several weeks needed for phase transition under quiescent condition, the transition rate is much faster by the aid of deformation, no matter what the temperature is. That is because the effect of deformation on the transformation is so large that the impact of temperature is minimized. In addition to the transition rate, different transition routes may occur at low and high temperatures, which also affects the transition rate at different temperatures and will be discussed below.

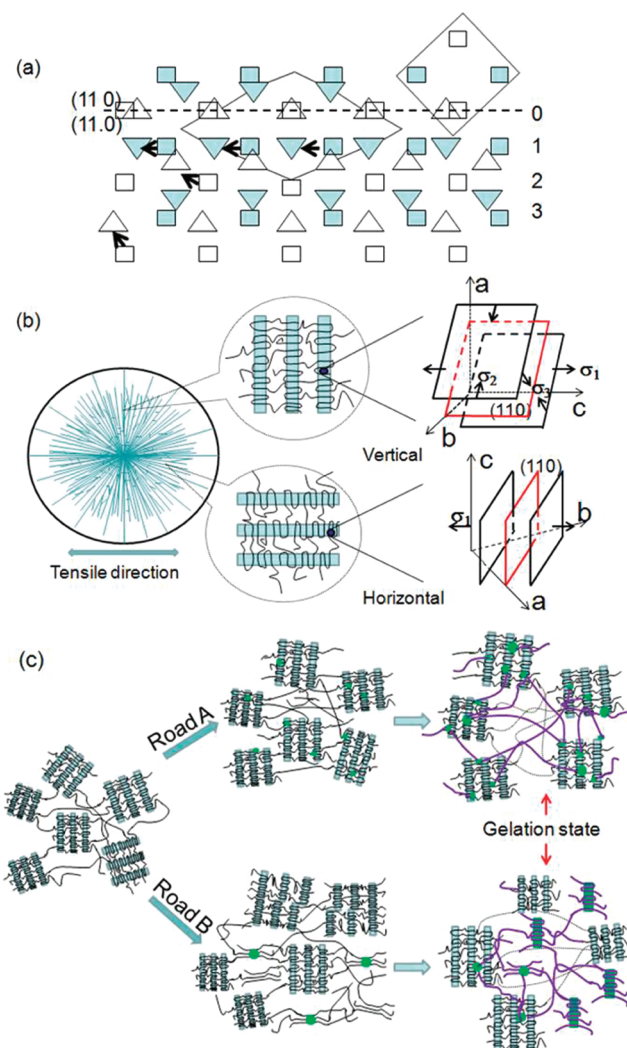


Figure 8. (a) Transformation scheme from forms II to I on the molecular level concerning with the “invariant plane” (110).⁴⁹ □ and △ represent 11_3 and 3_1 helices of forms II and I respectively. The different helical hands are shown as light and shaded. (b) Force condition of the planes (110) under uniaxial deformation in different zones of form II crystal. (c) Schematic diagrams for the gelation process of the form I mechanical network during the phase transition. A and B are the direct transformation from forms II to I and melting recrystallization process with melt as transient state, respectively. The blue and green blocks represent forms II and I crystal, respectively.

The evolution of the total crystallinity $X_{\text{II}+\text{I}}$ at different temperatures suggests that two different routes may be followed by the transition from forms II to I, as illustrated in Figure 8c. One is the direct transition from forms II to I, which takes place at quiescent condition and under tensile deformation at room temperature. Naturally another way is indirect transition from forms II to I with amorphous phase as the intermediate state. This indirect approach is rather plausible as evidenced by the evolution of crystallinity at high temperatures during tensile deformation. As shown in Figure 7a, the sum of crystallinity $X_{\text{II}+\text{I}}$ increases monotonically from about 43% to 52% at 25 °C. Here the increase of $X_{\text{II}+\text{I}}$ has two possible interpretations. (i) The remaining amorphous part in the initial samples crystallizes into form I directly under tensile deformation. (ii) The increase of $X_{\text{II}+\text{I}}$ may be due to larger crystalline diffraction intensities of form I than those of form II

with the same volume. If we take the first interpretation, the indirect transition approach from forms II to I with amorphous as the intermediate state can stand with further supports from the nonmonotonic evolution of X_{II+I} at 50 °C, which can be interpreted as a melting and recrystallization process. Now we take the second interpretation which means the crystalline diffractions of form I is much stronger than those of form II, so it can be assumed that the mass crystallinity is preserved during the transition from forms II to I at room temperature. With this scheme, the decrease of X_{II+I} in the first two stages (stage A and B) at 50 °C has to be attributed to melting of form II, while the increase of crystallinity in stage C is a recrystallization process, which confirms that the destruction of the original lamellae and recrystallization into new crystalline form occurs at the critical point C.³ The X_{II+I} at 80 °C follows a monotonic decrease, which also supports the idea of tensile deformation induced melting and recrystallization process. Thus, both direct and indirect transition approaches take place during tensile deformation induced transition from forms II to I, where the direct transition process may prefer at room temperature and the indirect one takes more shares at high temperature. These two approaches are in line with the two debated mechanisms on interpreting yield and orientation of crystalline polymers during tensile test. The direct transition from forms II to I mirrors Young and others' crystalline slip model, while the indirect transition with melting and recrystallization falls in the Flory–Yoon⁶⁶ approach, which, however, recrystallizes into stable form I instead of the initial metastable form II. Under continuous deformation, it is difficult to recrystallize into form II, because amorphous chains tend to orient in the tensile direction, while form II is reported to crystallize only from random chain conformation.⁴⁰ The structural evolution during tensile deformation shows clearly fingerprints on mechanical properties, which gives a nice demonstration on the correlation between phase transition and mechanical properties. At 25 and 50 °C, the appearance of form I exactly follows the yield point, where form II cannot sustain the tensile stress and coarse slip of lamellar crystal starts. In other words, yield point announces the aging of the parent phase form II, which is also the right point for the daughter phase form I to generate. At 80 °C, yield corresponds to tensile deformation induced melting of form II, which does not transform into form I immediately. Thus, for PB-1 samples with form II as the parent phase, the yield point corresponds to the starting point of phase transitions either from forms II to I at low temperature or from form II to melt at temperature close to melting point. Obviously, it coincides with a generalized view that the mechanism governing the process of tensile deformation of semicrystalline polymers at low and moderate deformations seems to be strain controlled. According to this model, block slips determine the yield points (point A and B),³ where nucleation of form I or melting of form II start. The second turning point in the engineering stress–strain curves leads to a strain hardening region, which takes place at relatively small strains (about 0.4) (Figure 1c and Figure 4, parts a and b). In the study of mechanical properties of other polyolefins, like polypropylene, polyethylene, polystyrene, etc. the strain hardening appears at larger strains (above 2).^{67,68} In semicrystalline polymer without the complication of phase transition, the molecular network plays an important role in the strain hardening, where crystal blocks start to destruct. In current case, strain hardening appears at relative small strain, which should not be attributed to stretched network. As the transition from forms II to I is the major

structural change in the stress plateau region before strain hardening, the stress level-up should be attributed to the formation of form I. Though the crystallinity of form I keeps relatively low (~5%) at the onset point of strain hardening, this is sufficient to establish a new mechanical network with form I crystals as physical cross-link if we compare the current system with physical gels. Indeed it is found that gelation of iPP melt during crystallization requires crystallinity of only 2% or less.⁶⁹ Though form I of PB-1 nucleates from a heterogeneous semicrystalline complex, the physical picture to construct the mechanical network should be similar to that in crystallization from melt. The difference here is that the initial network with form II as physical cross-link still exists though it can only sustain weak stress with a maximum of the plateau stress in the engineering stress–strain curves (see Figure 1c and Figure 4, parts a and b). In the stress plateau region, though form I crystals already appear, the concentration is low and they are dispersed in the heterogeneous matrix like suspensions without interaction among each other. Further increasing strain, the concentration of form I crystals increases, which finally reaches the gelation point with a crystallinity of about 5% (see Figure 8c). The formation of the new mechanical network contributes its role on sustaining stress, which reflects as strain hardening in the stress–strain curves.

CONCLUSIONS

Uniaxial tensile deformation induced the phase transition of PB-1 from forms II to I at different temperatures is investigated with *in situ* WAXS. The crystallinity evolution and orientation distribution of forms II and I show that the phase transformation is accelerated largely under tensile deformation. On the basis of the transition mechanism suggested by Fujiwara, the accelerating mechanism is deduced on the molecular level, as stretch could assist the interhelix and interplanar shrinkage of the “invariant plane” (110). Two phase transition routes are indicated in our experiment. The direct way from forms II to I may be dominant at low temperature, while the indirect one seems to be a process of deformation induced melting and recrystallization at high temperature. In the latter route, the metastable form II transforms into amorphous state due to uniaxial stretching at high temperature, which crystallizes into form I at large strain. The strain hardening takes place at a relatively small strain in uniaxial tensile deformation of PB-1, which is attributed to the mechanical network with form I crystal as the physical cross-link. A nice correlation between phase transition and mechanical property is established. The three stages of phase transformation, namely incubation, nucleation and gelation of form I, leave their signatures on the engineering stress–strain curve at different strain levels, respectively, reflecting as a three-stage mechanical behavior with linear deformation, stress plateau, and strain hardening.

AUTHOR INFORMATION

Corresponding Author

*E-mail: lqli@ustc.edu.cn.

Notes

The authors declare no competing financial interest.

ACKNOWLEDGMENTS

We would like to thank Prof. Wim H. de Jeu (Amherst), Prof. Bernard Lotz, and Dr. Bing Miao for helpful discussion, Prof. Guoqiang Pan and Dr. Zeming Qi for the assistance on WAXS

experiments, and Mr. Xiao Wang for the help on tensile tester. This work is supported by the National Natural Science Foundation of China (51033004, 50973103, 51120135002, 20904050), the Fund for One Hundred Talent Scientist of CAS, 973 program of MOST (2010CB934504), and the Doctoral Fund of MOE (200803580011). The research is also in part supported by the Opening Project of the State Key Laboratory of Polymer Materials Engineering (Sichuan University KF201001) and the State Key Laboratory of Polymer Physics and Chemistry (Changchun Institute of Applied Chemistry, CAS). We also would like to thank LyondellBasell Industries for providing PB-1 materials.

■ REFERENCES

- (1) Galeski, A. *Prog. Polym. Sci.* **2003**, *28*, 1643–1699.
- (2) Meijer, H. E. H.; Govaert, L. E. *Prog. Polym. Sci.* **2005**, *30*, 915–938.
- (3) Men, Y. F.; Rieger, J.; Strobl, G. *Phys. Rev. Lett.* **2003**, *91*, 095502/1–4.
- (4) Peterlin, A. *J. Mater. Sci.* **1971**, *6*, 490–508.
- (5) Lin, L.; Agron, A. *J. Mater. Sci.* **1994**, *29*, 294–323.
- (6) Samon, J. M.; Schultz, J. M.; Wu, J.; Hsiao, B. S.; Yeh, F.; Kolb, R. *J. Polym. Sci., Part B: Polym. Phys.* **1999**, *37*, 1277–1287.
- (7) Kawakami, D.; Ran, S. F.; Burger, C.; Avila-Orta, C.; Sics, I.; Chu, B.; Hsiao, B. S.; Kikutani, T. *Macromolecules* **2006**, *39*, 2909–2920.
- (8) Jiang, Z. Y.; Tang, Y. J.; Men, Y. F.; Enderle, H.; Lilge, D.; Roth, S. V.; Gehrke, R.; Rieger, J. *Macromolecules* **2007**, *40*, 7263–7269.
- (9) Men, Y. F.; Rieger, J.; Lindner, P.; Enderle, H. F.; Lilge, D.; Kristen, M. O.; Mihan, S.; Jiang, S. C. *J. Phys. Chem. B* **2005**, *109*, 16650–16657.
- (10) Kawakami, D.; Hsiao, B. S.; Ran, S. F.; Burger, C.; Fu, B.; Sics, I.; Chu, B.; Kikutani, T. *Polymer* **2004**, *45*, 905–918.
- (11) Kawakami, D.; Ran, S. F.; Christian, B.; Fu, B.; Sics, I.; Chu, B.; Hsiao, B. S. *Macromolecules* **2003**, *36*, 9275–9280.
- (12) Kawakami, D.; Christian, B.; Ran, S. F.; Avila-Orta, C.; Sics, I.; Chu, B.; Chiao, S. M.; Hsiao, B. S.; Kikutani, T. *Macromolecules* **2008**, *41*, 2859–2867.
- (13) Kakiage, M.; Yamanobe, T.; Komoto, T.; Murakami, S.; Uehara, H. *Polymer* **2006**, *47*, 8053–8060.
- (14) Wang, D. L.; Shao, C. G.; Zhao, B. J.; Bai, L. G.; Wang, X.; Yan, T. Z.; Li, J. J.; Pan, G. Q.; Li, L. B. *Macromolecules* **2010**, *43*, 2406–2412.
- (15) Bai, L. G.; Hong, Z. H.; Wang, D. L.; Li, J. J.; Wang, X.; Pan, G. Q.; Li, L. B.; Li, X. H. *Polymer* **2010**, *51*, 5604–5611.
- (16) Auriemma, F.; De Rosa, C. *Macromolecules* **2003**, *36*, 9396–9410.
- (17) Auriemma, F.; De Rosa, C.; Esposito, S.; Mitchell, G. R. *Angew. Chem., Int. Ed.* **2007**, *46*, 4325–4328.
- (18) Auriemma, F.; De Rosa, C. *J. Am. Chem. Soc.* **2006**, *128*, 11024–11025.
- (19) De Rosa, C.; Auriemma, F.; Di Capua, A.; Resconi, L.; Guidotti, S.; Gamurati, I.; Nifant'ev, I. E.; Laishevts, I. P. *J. Am. Chem. Soc.* **2004**, *126*, 17040–17049.
- (20) De Rosa, C.; Auriemma, F.; de Ballesteros, O. R.; Iacono, S. D.; De Luca, D.; Resconi, L. *Cryst. Growth Des.* **2009**, *9*, 165–176.
- (21) De Rosa, C.; Auriemma, F. *Lect. Notes Phys.* **2007**, *714*, 345–371.
- (22) Luciani, L.; Seppälä, J.; Löfgren, B. *Prog. Polym. Sci.* **1988**, *13*, 37–62.
- (23) De Rosa, C.; Auriemma, F.; Resconi, L. *Angew. Chem., Int. Ed.* **2009**, *48*, 9871–9874.
- (24) Luciani, L.; Seppälä, J.; Löfgren, B. *Prog. Polym. Sci.* **1988**, *13*, 37–62.
- (25) Natta, G.; Corradini, P.; Bassi, I. *Nuovo Cimento Suppl.* **1960**, *1*, 52–67.
- (26) Holland, V. F.; Miller, R. T. *J. Appl. Phys.* **1964**, *35*, 3241–3248.
- (27) Goldbach, G.; Peitscher, G. *Polym. Lett.* **1968**, *6*, 783–788.
- (28) Nakafuku, C.; Miyaki, T. *Polymer* **1983**, *24*, 141–148.
- (29) Turner-Jones, A. *Polymer* **1966**, *7*, 23–59.
- (30) Boor, J. Jr.; Mitchell, J. C. *J. Polym. Sci.: Part A* **1963**, *1*, 59–84.
- (31) Danusso, F.; Gianotti, G. *Makromol. Chem.* **1963**, *61*, 139–156.
- (32) Azzurri, F.; Flores, A.; Alfonso, G. C.; Baltá Calleja, F. J. *Macromolecules* **2002**, *35*, 9069–9073.
- (33) Azzurri, F.; Flores, A.; Alfonso, G. C.; Sics, I.; Hsiao, B. S.; Baltá Calleja, F. J. *Polymer* **2003**, *44*, 1641–1645.
- (34) Zhang, B.; Yang, D.; Yan, S. *J. Polym. Sci., Part B: Polym. Phys.* **2002**, *40*, 2641–2645.
- (35) Yamashita, M.; Ueno, S. *Cryst. Res. Technol.* **2007**, *42*, 1222–1227.
- (36) De Rosa, C. D.; Auriemma, F.; Ballesteros, O. R.; Esposito, F.; Laguzza, D.; Girolamo, R. D.; Resconi, L. *Macromolecules* **2009**, *42*, 8286–8297.
- (37) Jiang, Z. Y.; Sun, Y. Y.; Tang, Y. J.; Lai, Y. Q.; Funari, S. S.; Gehrke, R.; Men, Y. F. *J. Phys. Chem. B* **2010**, *114*, 6001–6005.
- (38) Miyoshi, T.; Hayashi, S.; Imashiro, F.; Kaito, A. *Macromolecules* **2002**, *35*, 2624–2632.
- (39) Lotz, B.; Thierry, A. *Macromolecules* **2003**, *36*, 286–290.
- (40) Nakamura, K.; Aoike, T.; Usaka, K.; Kanamoto, T. *Macromolecules* **1999**, *32*, 4975–4982.
- (41) Maruyama, M.; Sakamoto, Y.; Nozaki, K.; Yamamoto, T.; Kajikawa, H.; Toda, A.; Yamada, K. *Polymer* **2010**, *51*, 5532–5538.
- (42) Acieno, S.; Grizzuti, N.; Winter, H. H. *Macromolecules* **2002**, *35*, 5043–5048.
- (43) Fu, Q.; Heck, B.; Strobl, G.; Thomann, Y. *Macromolecules* **2001**, *34*, 2502–2511.
- (44) Men, Y. F.; Rieger, J.; Homeyer, J. *Macromolecules* **2004**, *37*, 9481–9488.
- (45) Chau, K. W.; Yang, Y. C.; Geil, P. H. *J. Mater. Sci.* **1986**, *21*, 3002–3014.
- (46) Al-Hussein, M.; Strobl, G. *Macromol. Symp.* **2004**, *214*, 231–240.
- (47) Jiang, S. D.; Duan, Y. X.; Li, L.; Yan, D. D.; Chen, E. Q.; Yan, S. K. *Polymer* **2004**, *45*, 6365–6374.
- (48) Marigo, A.; Marega, C.; Cecchin, G.; Collina, G.; Ferrara, G. *Eur. Polym. J.* **2000**, *36*, 131–136.
- (49) Fujiwara, Y. *Polym. Bull.* **1985**, *13*, 253–258.
- (50) Kopp, S.; Wittmann, J. C.; Lotz, B. *J. Mater. Sci.* **1994**, *29*, 6159–6166.
- (51) Armeniades, C. D.; Baer, E. *J. Macromol. Sci., Part B* **1967**, *1*, 309–334.
- (52) Li, L.; Liu, T.; Zhao, L.; Yuan, W. K. *Macromolecules* **2009**, *42*, 2286–2290.
- (53) Shi, J. Y.; Wu, P. Y.; Li, L.; Liu, T.; Zhao, L. *Polymer* **2009**, *50*, 5598–5604.
- (54) Tanaka, A.; Sugimoto, N.; Asada, T.; Onogi, S. *Polym. J.* **1975**, *7*, 529–537.
- (55) Sawai, D.; Anyashiki, T.; Nakamura, K.; Hisada, N.; Ono, T.; Kanamoto, T. *Polymer* **2007**, *48*, 363–370.
- (56) Samon, J. M.; Schultz, J. M.; Hsiao, B. S.; Wu, J.; Khot, S. J. *J. Polym. Sci., Part B: Polym. Phys.* **2000**, *38*, 1872–1882.
- (57) Kaszonyiova, M.; Rybníkář, F.; Geil, P. H. *J. Macromol. Sci., Phys.* **2004**, *B43*, 1095–1114.
- (58) Schaffhauser, R. J. *J. Polym. Sci., Part B: Polym. Lett.* **1967**, *5*, 839–841.
- (59) Goldbach, G. *Angew. Makromol. Chem.* **1973**, *29*, 213–227.
- (60) Yang, Y. C.; Geil, P. H. *Makromol. Chem.* **1985**, *186*, 1961–1978.
- (61) Bowden, P. B.; Jukes, J. A. *J. Mater. Sci.* **1972**, *7*, 52–63.
- (62) Wu, J. B. C.; Li, J. C. M. *J. Mater. Sci.* **1972**, *11*, 434–444.
- (63) Bowden, P. B.; Young, R. J. *J. Mater. Sci.* **1974**, *9*, 2034–2051.
- (64) Bartczak, Z.; Argon, A. S.; Cohen, R. E. *Macromolecules* **1992**, *25*, 5036–5053.
- (65) Gohil, R. M.; Miles, M. J.; Petermann, J. *J. Macromol. Sci. Phys.* **1982**, *B21*, 189–201.
- (66) Flory, P. J.; Yoon, D. Y. *Nature* **1978**, *272*, 226–229.
- (67) Kennedy, M. A.; Peacock, A. J.; Mandelkern, L. *Macromolecules* **1994**, *27*, 5297–5310.

(68) Nitta, K.; Ishiburo, T. *J. Polym. Sci., Part B: Polym. Phys.* **2002**, *40*, 2018–2026.

(69) Pogodina, N. V.; Winter, H. H. *Macromolecules* **1998**, *31*, 8164–8172.